

# Mid-Latitude Jet Response to Pan-Arctic and Regional Arctic Warming in Idealized GCM

Gun-Hwan Yang, Woosok Moon, Hayeon Noh and Baek-Min Kim \*

Division of Earth Environmental System Science, Major of Environmental Atmospheric Sciences, Pukyong National University, Busan 48513, Republic of Korea

\* Correspondence: baekmin@pknu.ac.kr

**Abstract:** To study the dynamical mechanism by which Arctic amplification affects extreme weather events in mid-latitude, we investigated the local and remote circulation response to pan-Arctic and regional Arctic thermal forcing. A comprehensive atmospheric GCM (General Circulation Model) coupled to a slab mixed-layer ocean model is used for the experiment. With the increasing thermal forcing in the pan-Arctic configuration, the mid-latitude jet tends to shift equatorward, mainly due to the southward shift of the convergence zone of eddy-heat flux and eddy-momentum flux. From the regional Arctic forced experiments, zonal mean response is similar to the response from the pan-Arctic configuration. The non-zonal response is characterized by the 300 hPa circumpolar zonal wind of wavenumber-1 structure, which establishes an enhanced wavier mid-latitude jet. In the polar region at 300 hPa, regional thermal forcing drives a distinct east–west dipole circulation pattern, in which anticyclonic circulation is located to the west of the thermal forcing, and cyclonic circulation is located to the east. The lower-level circulation shows the opposite pattern to the upper-level circulation in the polar region. While the strength of circulation increases with gradual thermal forcing, the overall dipole pattern is unchanged. In regional warming simulation, compared to the pan-Arctic warming, increasing residual heat flux in a dipole pattern causes enhanced heat advection to mid-latitude.

**Keywords:** Arctic amplification; atmospheric circulation; jet; climate change; idealized model



**Citation:** Yang, G.-H.; Moon, W.; Noh, H.; Kim, B.-M. Mid-Latitude Jet Response to Pan-Arctic and Regional Arctic Warming in Idealized GCM. *Atmosphere* **2023**, *14*, 510. <https://doi.org/10.3390/atmos14030510>

Academic Editors: Sridhara Nayak and Netrananda Sahu

Received: 3 January 2023

Revised: 21 February 2023

Accepted: 27 February 2023

Published: 6 March 2023



**Copyright:** © 2023 by the authors. Licensee MDPI, Basel, Switzerland. This article is an open access article distributed under the terms and conditions of the Creative Commons Attribution (CC BY) license (<https://creativecommons.org/licenses/by/4.0/>).

## 1. Introduction

Under the warming climate, extreme weather events in mid-latitude such as cold surges and heat waves have increased in frequency and intensity in the Northern Hemisphere [1,2]. In the Arctic region, the ocean, cryosphere, and atmosphere interact with various and complex physical processes. Strong feedback processes among these climate components in the Arctic accelerate the warming over the Arctic region more than four times as fast as the global average [3]. In addition, dynamical pathways and propagation involving the polar vortex, jet stream, and Arctic oscillation tend to link the Arctic and mid-latitude climate [4–7]. However, uncertainty in the model and insufficient observations make it difficult to understand the cause of the Arctic–Mid-latitude teleconnection [8,9]. Arctic amplification essentially shows regional structure. Surface temperature increase is more pronounced over marginal ice zones such as the Barents/Kara Seas and Chukchi Seas, where the rapid decrease of ice is observed [10,11]. Previous studies have conducted GCM (General Circulation Model) simulation, prescribing the reduced sea ice in the Arctic and examining the atmospheric teleconnection related to the Arctic sea ice loss [5,10,12]. Despite several modeling studies, the effects of Arctic sea ice loss, such as localized feedback or teleconnection, are unclear. Complex physical processes involving cloud, sea ice, and cryosphere–atmosphere interaction induce considerable uncertainty in the parameterization of GCM. To focus on the fundamental issue related to the characteristic differences in the pan-Arctic versus regional Arctic warming, we examined the atmospheric response to both pan-Arctic and regional surface heating with an idealized modeling experiment.

According to the previous studies, Arctic surface warming or a decrease in the meridional temperature gradient results in the weakening of upper zonal wind in mid-latitude [13,14]. In addition, a decrease of the meridional temperature gradient causes the weakening of Hadley circulation and shifts the ITCZ (intertropical convergence zone), resulting in a significant change in the meridional energy transport [15]. The decline in the meridional temperature gradient, accompanied by a stationary wave, shifts the baroclinic zone towards the equator [16]. Additionally, stratospheric warming changes the location of the jet stream and intensifies its strength [17]. The additional thermal forcing in the mid-latitudes results in a zonal temperature contrast due to the stationary Rossby wave [18].

We investigate the idealized atmospheric response in the Arctic region and Arctic–Mid-latitude teleconnection produced by Arctic thermal forcing. For this purpose, we conduct the idealized GCM with zonally symmetric and asymmetric thermal forcing. Each thermal forcing represents the strength and shape of the Arctic amplification. To investigate the responses to the given forcing, we analyze variables characterizing circulation, radiation, and fluxes in both zonal mean and zonally asymmetric parts. We also analyze the surface energy balance changes and stationary wave response by thermal forcing.

In Section 2, we briefly describe the idealized GCM, including previous studies that used the model. Section 2 also explains the experimental design of the idealized model. Section 3 describes the main results from the numerical model experiment. In Section 4, we summarize the results.

## 2. Materials and Methods

### 2.1. Model Description

To analyze the response to Arctic warming, the model employed in this study is the simplified moist GCM of Frierson et al. [19] provided by the Geophysical Fluid Dynamics Laboratory (GFDL). The model uses primitive equations with a simplified hydrological cycle. The long-wave physics are gray radiative transfer, in which radiative fluxes are only a function of temperature. There are no water vapor and cloud feedback effects. The long-wave optical depth approximates the effects of water vapor. In convection parameterization, large-scale condensation and a simplified Betts–Miller connection scheme were used. The lower boundary is an aquaplanet slab mixed layer ocean. Surface diffusion coefficients within the boundary layer are calculated in accordance with the simplified Monin–Obukhov theory. For details, see Frierson et al. [19].

The model, with a hydrocycle and convection scheme, simulates a more realistic equatorial climate than the dry idealized atmospheric model, while maintaining the characteristics of the simplified model [19,20]. Furthermore, this model can control static stability, energy transport, and planetary boundary height sensitivity by varying relative humidity conditions. This model has been mainly used for basic research on climate change in equatorial regions, such as strength and width of Hadley circulation and ITCZ [15,21,22], and for research on zonal wind and jet stream changes in mid-latitude areas [14,23]. The model has also been used to study the changes in the upper zonal mean and stationary waves by prescribing zonally asymmetric thermal forcing [16,18].

### 2.2. Experiment Set-Up

In this study, we impose thermal forcing (Q-flux) on the model to simulate Arctic warming. To represent pan-Arctic warming, thermal forcing in high-latitude ( $70^{\circ}$  N– $90^{\circ}$  N,  $0^{\circ}$  E– $360^{\circ}$  E) is prescribed, with the experiments referred to as ‘CASE 1 (C1)’. We vary Q-flux in C1 from  $15 \text{ W m}^{-2}$  to  $85 \text{ W m}^{-2}$  in increments of  $10 \text{ W m}^{-2}$ , referred to as ‘C1-HF1’ to ‘C1-HF8’ (Table S1). To mimic the thermal forcing driven by sea ice loss over the Barents/Kara Seas or Chukchi Sea, we impose local thermal forcing ( $70^{\circ}$  N– $90^{\circ}$  N,  $0^{\circ}$  E– $360^{\circ}$  E) in the idealized GCM and refer to the experiments as ‘CASE2 (C2)’. We vary Q-flux in C2 from  $90 \text{ W m}^{-2}$  to  $510 \text{ W m}^{-2}$  in increments of  $60 \text{ W m}^{-2}$  and refer to the experiments as ‘C2-HF1’ to C2-HF8’ (Table S1).

Because the area of forcing region in the C2 experiments is six times smaller than in the C1 experiments, we apply the same amount of total energy for fair comparison by applying six times stronger Q-flux in the C2 experiments than in the C1 experiments. For the comparison, a no-forcing experiment is also prepared and referred to as the control experiment (CTRL). All experiments are integrated with T42 (approximately  $2.5^\circ \times 2.5^\circ$ ) horizontal resolution and 25 layers of the vertical sigma levels. The model is integrated for 14,400 days for every experiment, and the last 7200 days are averaged.

In this study, estimation of the exact location of the mid-latitude jet is in accordance with Adam et al. [24] (Equation (1)). In Equation (1),  $F(\phi)$  is a zonally averaged field, and  $\phi_{\max}$  is the latitude where the variable  $F$  has the maximum value.  $\phi_1$  and  $\phi_2$  are meridional boundaries, and  $n$  is a smoothing parameter. The position of the mid-latitude jet is defined as the latitude of the maximum 850 hPa zonally averaged wind field. In control the experiment, the position of mid-latitude jet is located at about  $40^\circ$  N.

$$\phi_{\max} = \int_{\phi_1}^{\phi_2} F(\phi)^n \phi d\phi / \int_{\phi_1}^{\phi_2} F(\phi)^n d\phi, \quad (1)$$

### 3. Results

#### 3.1. Thermal and Dynamical Response from Pan-Arctic Forcing

First, we investigate the atmospheric impacts of the incremental intensification of the surface thermal forcing (Q-flux) in polar regions ( $70^\circ$  N– $90^\circ$  N). As expected, the response to polar surface forcing shows the most noticeable warming in the polar lower atmosphere. Surface temperature in the polar region increases about 1–3 K in C1-HF1 (not shown), 7–9 K in C1-HF4, and approximately 13–15 K in C1-HF8 (Figure 1a,b). A linear relationship exists between the thermal forcing and surface temperature, indicating that the thermal forcing influences the change of the mid-latitude jet through thermal wind balance. Based on the mid-latitude jet in CTRL, the zonal wind decreases in a poleward direction and increases in an equatorward direction (Figure 1c,d).

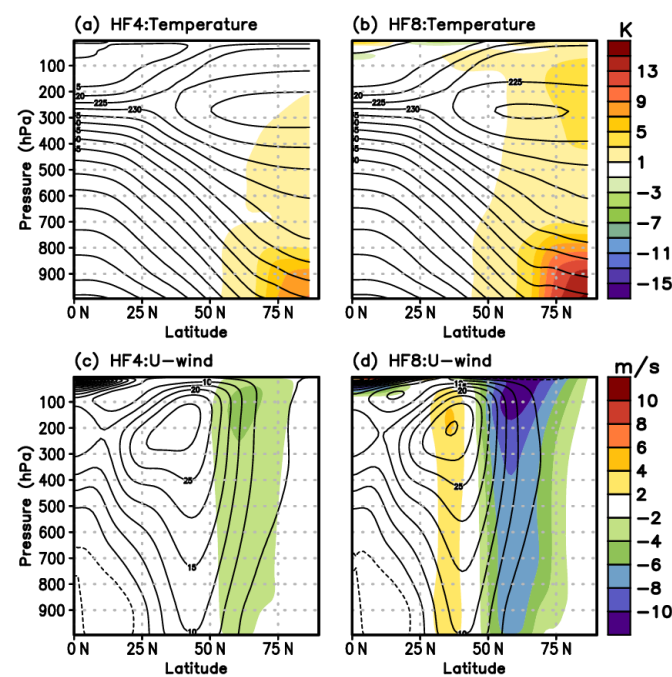


**Figure 1.** Time-mean zonally averaged (a,b) temperature (contours) and deviation (shaded) from control experiment, contour intervals are 10 K, and (c,d) zonal wind (contours) and deviation (shaded) from control experiment, contour intervals are 5 m/s.

The experiments do not consider complex parameterization processes such as cloud and sea ice physics. However, the idealized GCM uses incoming shortwave radiation and a

simplified longwave radiation scheme. Moreover, the lower-boundary condition simulates the energy balance equation. The processes represent the response from additional thermal flux at the surface (Figure 2).

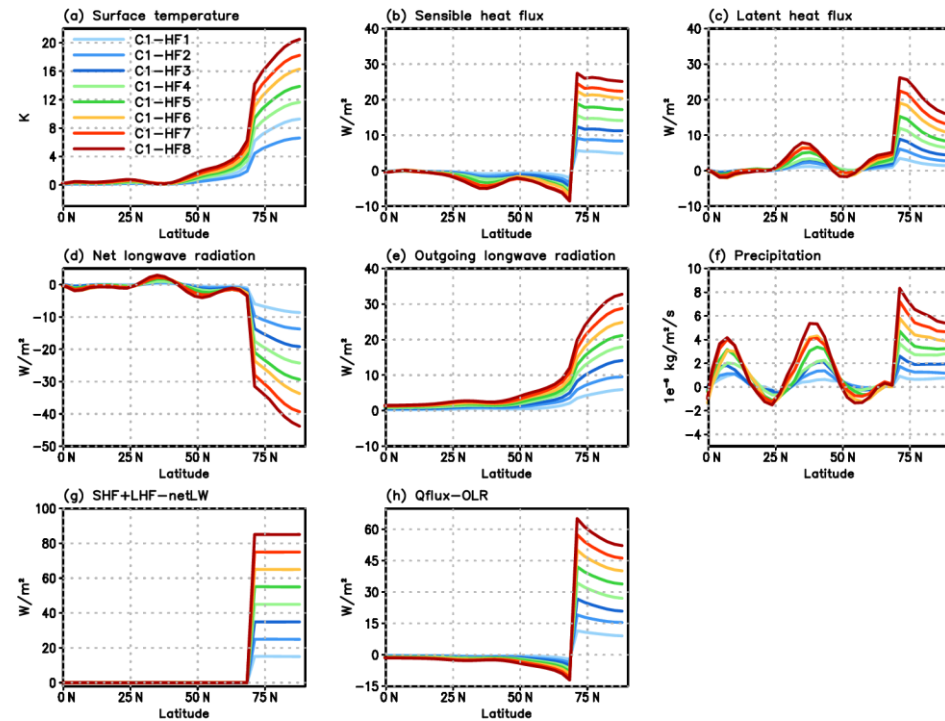


**Figure 2.** Time-mean zonally averaged deviation from CTRL (a) surface temperature, (b) sensible heat flux, (c) latent heat flux, (d) net downward longwave radiation, (e) outgoing longwave radiation, (f) precipitation, (g) surface energy balance, (h) difference between surface thermal forcing and outgoing longwave radiation.

As thermal forcing leads to increased surface temperature in the polar region (70° N) (Figure 2a), the amount of sensible heat, latent heat, and net long-wave radiation increases, emitted from the surface (Figure 2b–d). In surface energy balance, the sum of the sensible heat flux, latent heat flux, and net long-wave radiation equals the total prescribed thermal forcing. There is no additional heat flux generated through the feedback process (Figure 2g). Additionally, an increase in latent heat leads to an increase in precipitation (Figure 2f). Outgoing long-wave radiation (OLR) increases as the surface temperature increases (Figure 2e), but the increment is not sufficient for the prescribed thermal forcing. Therefore, the residual heat migrates towards the mid-latitude region (Figure 2h). In the mid-latitude region, the surface temperature increases, but the sensible heat flux tends to decrease, in contrast to the polar region. The warming of the mid-latitude region is caused by warm advection from the polar region. To maintain the surface energy balance in the mid-latitude, the OLR and latent heat flux increase. This leads to an increase in precipitation in the 25° N to 50° N region, as the latent heat flux increases (Figure 2).

As the meridional temperature gradient in the northern hemisphere decreases, the Hadley circulation weakens. This is characterized by increasing lower-level meridional winds and decreasing upper-level meridional winds in the tropics (0° N–40° N) (Figure 3a,b). The results appear to be similar to those suggested by Kang et al. [15], where the meridional temperature gradient is compensated by a shift in the Hadley circulation. The increase in temperature in the polar region results in a decrease in the eddy heat flux around 850 hPa in the 70° N region and the eddy momentum flux around 400 hPa in the 50° N region. As a result of the shift in the divergence of the Eliassen-Palm flux towards the equator, the mid-latitude jet also shifts towards the equator (Figure 3c,d). In addition, eddy momentum flux and eddy heat flux changes weaken the Ferrel cell circulation. The weakening of the

Ferrel cell circulation leads to decreased lower-level meridional winds and increased upper-level meridional winds in the mid-latitude ( $50^{\circ}\text{N}$ – $70^{\circ}\text{N}$ ). As the eddy heat flux decreases through a change of meridional wind around  $70^{\circ}\text{N}$ , the poleward eddy moisture flux decreases (not shown). The change of meridional wind, in the high-latitude and low-latitude drives the convergence of moisture and rainfall in mid-latitude (Figure 2f).

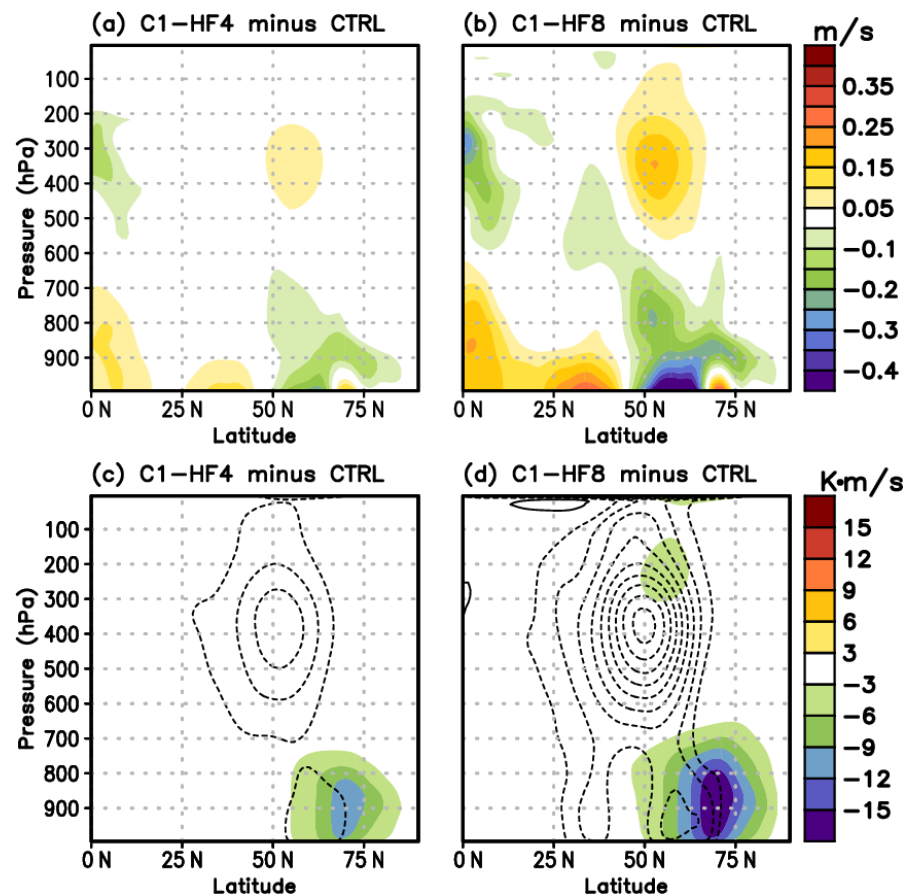


**Figure 3.** Time-mean zonally averaged (a,b) meridional wind deviation (shaded) from control experiment, (c,d) transient eddy momentum flux deviation (contours) and transient eddy heat flux deviation (shaded) from control experiment; contour intervals are  $2\text{ m}^2/\text{s}^2$ .

In our study, we examine the changes in the general circulation, eddy fluxes, and mid-latitude jet. The pan-Arctic thermal forcing in the polar regions drives a reduction in the meridional temperature gradient and the transport of residual energy. This results in the decrease of eddy heat flux and thermal wind balance, leading to a weakening of the mid-latitude jet and Ferrel cell. The decline of the Hadley circulation leads to a decrease in eddy momentum flux and the strength of the mid-latitude jet. However, as shown in Figure 1d, the mid-latitude jet shifts towards the equator and compounds with the subtropical jet. The interaction between the mid-latitude and high-latitude regions primarily drives the changes in the mid-latitude jet.

### 3.2. Thermal and Dynamical Response from Regional Arctic Forcing

To represent the impact of sea ice loss on stationary wave patterns, we impose the regional thermal forcing in the polar region. Centered on CTRL's mid-latitude jet (purple line in Figure 4), the mid-latitude jet shifts toward the equator in the longitude area where regional forcing is imposed ( $0^{\circ}\text{E}$ – $60^{\circ}\text{E}$ ), and the mid-latitude jet shifts northward, eastward of regional forcing ( $80^{\circ}\text{E}$ – $140^{\circ}\text{E}$ ) (Figure 4a,b). The deviation of the zonal wind strengthens in proportion to the magnitude of the additional thermal forcing, and there is no significant difference in the pattern. The wavier mid-latitude jet at 300 hPa

propagates at the lower level, resulting in a similar pattern of the zonal wind at 850 hPa (30° N–60° N). The additional forcing, located at the surface, influences the mid-latitude surface condition. However, in mid-latitude, the deviation of zonal wind at 850 hPa is weaker than at 300 hPa (Figure 4).

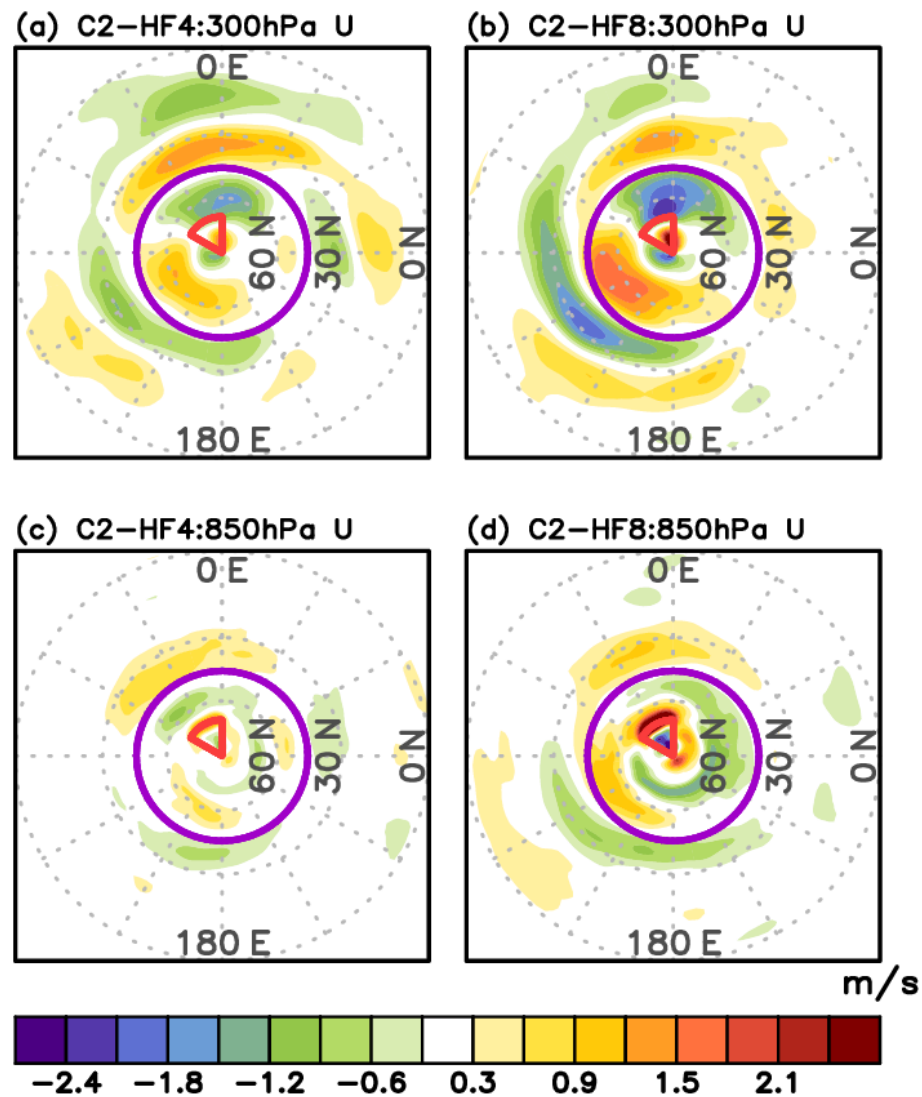


**Figure 4.** Time-mean zonal deviation: (a,b) 300 hPa zonal wind (shaded, unit: m/s), (c,d) 850 hPa zonal wind (shaded, unit: m/s). The purple solid line is CTRL's eddy-driven jet position, and the red triangle represents the area of prescribing Q-flux.

In the 300 hPa, a cyclonic circulation locates where the mid-latitude jet shifts southward, and an anticyclonic circulation locates where the mid-latitude jet shifts northward (Figures 4 and 5). In the polar region at 300 hPa, an anticyclonic circulation locates westward of the Q-flux, while a cyclonic circulation is located eastward. On the eastside of the thermal forced region, The east-west dipole circulation pattern strengths northerly wind. The lower-level circulation in the polar region shows the opposite pattern to the upper-level circulation. The zonal wind and stream function deviation increase in proportion to the strength of the thermal forcing, and the location is not significantly different. However, the meridional wind deviation is not proportional to the forcing, and the pattern is different by strength of forcing (not shown).

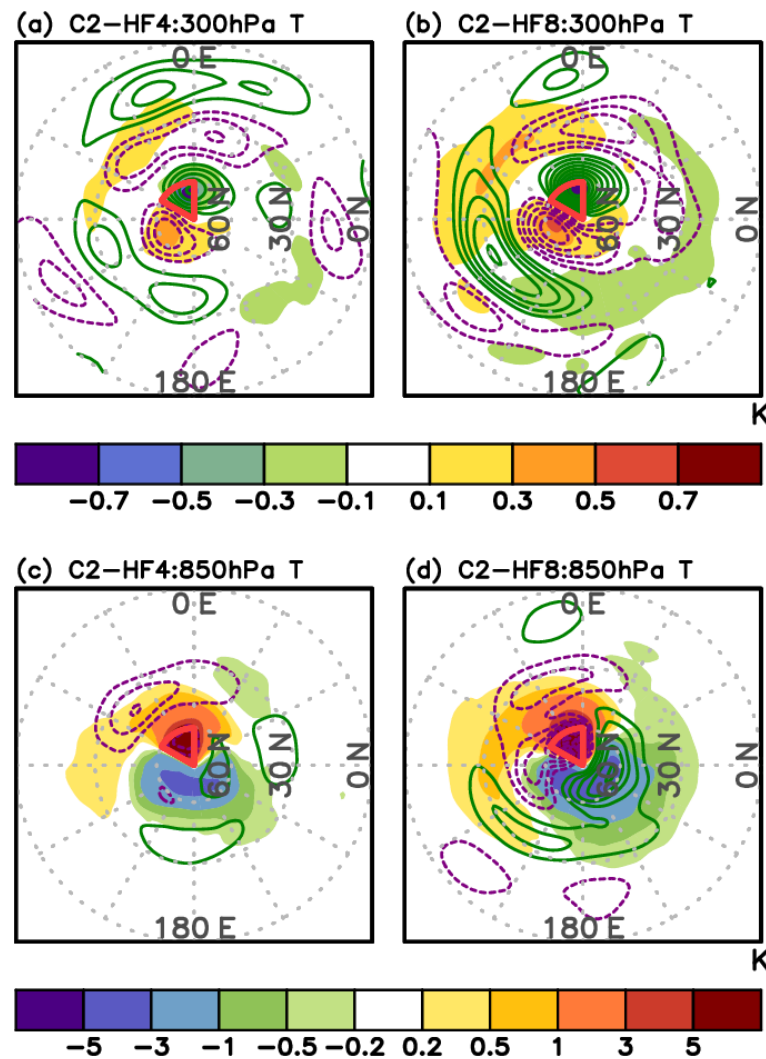


**Figure 5.** Time-mean zonal deviation: (a,b) 300 hPa temperature (shaded, unit: K) and stream function (contours,  $4 \times 10^5 \text{ m}^2/\text{s}$ ); (c,d) 850 hPa temperature (shaded, unit: K) and stream function (contours,  $4 \times 10^5 \text{ m}^2/\text{s}$ ). Purple contours are negative, and green contours are positive. The red triangle represents the area of prescribing Q-flux.

The temperature change in the polar region drives lower-level cyclonic circulation and upper-level anticyclonic circulation with upstream motion (Figure 5). Upstream motion induces diabatic cooling, driving negative temperature deviation. The warm deviation in the lower-level mid-latitude is driven by the warm advection from the polar region and the westerly wind. The warm deviation in the upper level is generated by the meridional wind that is exhibited between the trough and ridge (Figure 5).

As a result, the enhancement of the wavenumber-1 stationary wave structure in mid-latitude strengthens the baroclinicity. In the polar region, the upstream motion leads to the circulation change from the surface. However, in mid-latitude, the upper level circulation change is propagated to the lower level.

#### 4. Discussion

This study investigates the unique atmospheric responses to both zonally symmetric and asymmetric Arctic surface heating using an idealized GCM. Our results show that the zonally symmetric heating in the Arctic yields similar outcomes to previous studies [15]. However, the results represent relatively fewer significant changes in the Hadley circulation and a more confined response at mid-latitude and the polar region. Meanwhile, the zonally

asymmetric heating experiment, representing the recent abrupt decrease of sea ice over specific marginal ice zones, leads to the formation of an east-west dipole circulation pattern in the polar region and a wavier stationary wave in mid-latitude.

Our findings are consistent with previous studies using GCMs and reanalysis data to investigate the impact of snow decline or sea ice loss [5,10,25]. However, the effect of localized warming is not confined the response of sea ice loss and snow. The anomalous warming in high-latitude, such as wildfire, negative northern annular mode, inflow of storm, leads to the wavenumber-1 component of stationary wave and jet stream. In turn, the meandering mid-latitude jet can drive extreme event in mid-latitude such as cold surge, blocking, drought or heavy rain fall.

We used the simplest GCM, does not account for complex parameterization, such as land, sea ice, cloud, and longwave radiation flux processes. The complex processes can amplify or decline the diabatic thermal forcing and instability, and to fully comprehend the effect of stratospheric circulation, we must also consider the dynamics of ozone. Further studies using both simple and realistic models are needed to analyze the feedback mechanisms and to improve our understanding of the Arctic-midlatitude linkage.

**Supplementary Materials:** The following supporting information can be downloaded at: <https://www.mdpi.com/article/10.3390/atmos14030510/s1>, Table S1: Strength of Q-flux.

**Author Contributions:** Conceptualization and supervision, B.-M.K.; formal analysis, G.-H.Y.; writing review and editing, W.M. and H.N.; All authors have read and agreed to the published version of the manuscript.

**Funding:** This work was supported by Korea Environment Industry & Technology Institute (KEITI) through “Climate Change R&D Project for New Climate Regime.” This research was funded by the Korea Ministry of Environment (MOE) (RE202201655).

**Institutional Review Board Statement:** Not applicable.

**Informed Consent Statement:** Not applicable.

**Data Availability Statement:** The idealized model is described in this paper.

**Conflicts of Interest:** The authors declare no conflict of interest.

## References

1. Johnson, N.C.; Xie, S.P.; Kosaka, Y.; Li, X. Increasing Occurrence of Cold and Warm Extremes during the Recent Global Warming Slowdown. *Nat. Commun.* **2018**, *9*, 1724. [[CrossRef](#)] [[PubMed](#)]
2. Perkins-Kirkpatrick, S.E.; Lewis, S.C. Increasing Trends in Regional Heatwaves. *Nat. Commun.* **2020**, *11*, 3357. [[CrossRef](#)] [[PubMed](#)]
3. Rantanen, M.; Karpechko, A.Y.; Lipponen, A.; Nordling, K.; Hyvärinen, O.; Ruosteenoja, K.; Vihma, T.; Laaksonen, A. The Arctic Has Warmed Nearly Four Times Faster than the Globe since 1979. *Commun. Earth Environ.* **2022**, *3*, 168. [[CrossRef](#)]
4. Cohen, J.; Zhang, X.; Francis, J.; Jung, T.; Kwok, R.; Overland, J.; Ballinger, T.J.; Bhatt, U.S.; Chen, H.W.; Coumou, D.; et al. Divergent Consensuses on Arctic Amplification Influence on Midlatitude Severe Winter Weather. *Nat. Clim. Chang.* **2020**, *10*, 20–29. [[CrossRef](#)]
5. Kim, B.M.; Son, S.W.; Min, S.K.; Jeong, J.H.; Kim, S.J.; Zhang, X.; Shim, T.; Yoon, J.H. Weakening of the Stratospheric Polar Vortex by Arctic Sea-Ice Loss. *Nat. Commun.* **2014**, *5*, 4646. [[CrossRef](#)]
6. Polvani, L.M.; Waugh, D.W. Upward Wave Activity Flux as a Precursor to Extreme Stratospheric Events and Subsequent Anomalous Surface Weather Regimes. *J. Clim.* **2004**, *17*, 3548–3554. [[CrossRef](#)]
7. Xie, Y.; Wu, G.; Liu, Y.; Huang, J.; Nie, H. A Dynamic and Thermodynamic Coupling View of the Linkages between Eurasian Cooling and Arctic Warming. *Clim. Dyn.* **2022**, *58*, 2725–2744. [[CrossRef](#)]
8. Blackport, R.; Screen, J.A.; van der Wiel, K.; Bintanja, R. Minimal Influence of Reduced Arctic Sea Ice on Coincident Cold Winters in Mid-Latitudes. *Nat. Clim. Chang.* **2019**, *9*, 697–704. [[CrossRef](#)]
9. Blackport, R.; Screen, J.A. Weakened Evidence for Mid-Latitude Impacts of Arctic Warming. *Nat. Clim. Change* **2020**, *10*, 1065–1066. [[CrossRef](#)]
10. Kug, J.S.; Jeong, J.H.; Jang, Y.S.; Kim, B.M.; Folland, C.K.; Min, S.K.; Son, S.W. Two Distinct Influences of Arctic Warming on Cold Winters over North America and East Asia. *Nat. Geosci.* **2015**, *8*, 759–762. [[CrossRef](#)]
11. Screen, J.A.; Simmonds, I. Increasing Fall-Winter Energy Loss from the Arctic Ocean and Its Role in Arctic Temperature Amplification. *Geophys. Res. Lett.* **2010**, *37*, 16707. [[CrossRef](#)]

12. Mori, M.; Watanabe, M.; Shiogama, H.; Inoue, J.; Kimoto, M. Robust Arctic Sea-Ice Influence on the Frequent Eurasian Cold Winters in Past Decades. *Nat. Geosci.* **2014**, *7*, 869–873. [[CrossRef](#)]
13. Butler, A.H.; Thompson, D.W.J.; Heikes, R. The Steady-State Atmospheric Circulation Response to Climate Change-like Thermal Forcings in a Simple General Circulation Model. *J. Clim.* **2010**, *23*, 3474–3496. [[CrossRef](#)]
14. Lu, J.; Chen, G.; Frierson, D.M.W. The Position of the Midlatitude Storm Track and Eddy-Driven Westerlies in Aquaplanet AGCMs. *J. Atmos. Sci.* **2010**, *67*, 3984–4000. [[CrossRef](#)]
15. Kang, S.M.; Frierson, D.M.W.; Held, I.M. The Tropical Response to Extratropical Thermal Forcing in an Idealized GCM: The Importance of Radiative Feedbacks and Convective Parameterization. *J. Atmos. Sci.* **2009**, *66*, 2812–2827. [[CrossRef](#)]
16. Shin, Y.; Kang, S.M.; Watanabe, M. Dependence of Arctic Climate on the Latitudinal Position of Stationary Waves and to High-Latitudes Surface Warming. *Clim. Dyn.* **2017**, *49*, 3753–3763. [[CrossRef](#)]
17. Lee, J.; Son, S.; Kim, S.; Song, K. The Sensitivity of the Extratropical Jet to the Stratospheric Mean State in a Dynamic-Core General Circulation Model. *Atmosphere* **2021**, *31*, 171–183.
18. Kaspi, Y.; Schneider, T. Winter Cold of Eastern Continental Boundaries Induced by Warm Ocean Waters. *Nature* **2011**, *471*, 621–624. [[CrossRef](#)]
19. Frierson, D.M.W.; Held, I.M.; Zurita-Gotor, P. A Gray-Radiation Aquaplanet Moist GCM. Part I: Static Stability and Eddy Scale. *J. Atmos. Sci.* **2006**, *63*, 2548–2566. [[CrossRef](#)]
20. Frierson, D.M.W.; Held, I.M.; Zurita-Gotor, P. A Gray-Radiation Aquaplanet Moist GCM. Part II: Energy Transports in Altered Climates. *J. Atmos. Sci.* **2007**, *64*, 1680–1693. [[CrossRef](#)]
21. Frierson, D.M.W.; Lu, J.; Chen, G. Width of the Hadley Cell in Simple and Comprehensive General Circulation Models. *Geophys. Res. Lett.* **2007**, *34*, 1–5. [[CrossRef](#)]
22. Kang, S.M.; Held, I.M.; Frierson, D.M.W.; Zhao, M. The Response of the ITCZ to Extratropical Thermal Forcing: Idealized Slab-Ocean Experiments with a GCM. *J. Clim.* **2008**, *21*, 3521–3532. [[CrossRef](#)]
23. Hell, M.C.; Schneider, T.; Li, C. Atmospheric Circulation Response to Short-Term Arctic Warming in an Idealized Model. *J. Atmos. Sci.* **2020**, *77*, 531–549. [[CrossRef](#)]
24. Adam, O.; Grise, K.; Staten, P.; Simpson, I.; Davis, S.; Davis, N.; Waugh, D.; Birner, T. The TropD Software Package: Standardized Methods for Calculating Tropical Width Diagnostics. *Geosci. Model Dev.* **2018**, *11*, 4339–4357. [[CrossRef](#)]
25. Cohen, J.; Barlow, M.; Kushner, P.J.; Saito, K. Stratosphere-Troposphere Coupling and Links with Eurasian Land Surface Variability. *J. Clim.* **2007**, *20*, 5335–5343. [[CrossRef](#)]

**Disclaimer/Publisher’s Note:** The statements, opinions and data contained in all publications are solely those of the individual author(s) and contributor(s) and not of MDPI and/or the editor(s). MDPI and/or the editor(s) disclaim responsibility for any injury to people or property resulting from any ideas, methods, instructions or products referred to in the content.